PHOTOACOUSTIC PHOTOCALORIMETRY AND SPECTROSCOPY OF *HALOBACTERIUM HALOBIUM* PURPLE MEMBRANES

HAIM GARTY AND S. ROY CAPLAN
Department of Membrane Research, Weizmann Institute of Science, Rehovot, Israel
DAVID CAHEN
Department of Structural Chemistry, Weizmann Institute of Science, Rehovot, Israel

ABSTRACT Enthalpy changes associated with intermediates of the photocycle of bacteriorhodopsin (bR) in light-adapted *Halobacterium halobium* purple membranes, and decay times of these intermediates, are obtained from photoacoustic measurements on purple membrane fragments. Our results, mainly derived from modulation frequency spectra, show changes in the amount of energy stored in the intermediates and in their decay times as a function of pH and/or salt concentration. Especially affected are the slowest step (endothermic) and a spectroscopically unidentified intermediate (both at pH 7). This effect is interpreted in terms of cation binding to the protein, conformational changes of which are thought to be connected with the endothermic process. Wavelength spectra are used to obtain heat dissipation spectra, which allow identification of wavelength regions with varying photoactivity, and estimation of the amounts of enthalpy stored in the photointermediates. Because of bleaching and accumulation of intermediates, however, and because of the small fraction of light energy stored during photocycle, quantitative information cannot be obtained. From photoacoustic wavelength spectra of purple membrane fragments equilibrated at 63% relative humidity, rise and decay times of the bR_{570} and M_{412} intermediates are calculated.

INTRODUCTION

The purple membrane of *Halobacterium halobium*, which functions as a light-driven proton pump, has been studied intensively during the last decade (for reviews see references 1 and 2). Some of the reasons for the interest in this system are (*a*) its simplicity as compared with other bioenergetic systems, (*b*) the similarity between the photochemical processes occurring in it and those that take place in rhodopsin during the visual process, and (*c*) its functional stability. Purple membrane contains a simple protein, bacteriorhodopsin (bR), to which a retinal molecule is attached. Absorption of light by the retinal moiety causes (after an initial light adaptation) a series of cyclic absorption changes that, in the case of a pulse, are terminated after ~10 ms. During this photocycle, protons are translocated from the cytoplasmic to the external side of the membrane. Although a great deal of information on the photocycle has been obtained, fundamental questions concerning the conversion of visible light into chemical energy by bR remain. We shall address ourselves to one of these questions here, namely the magnitude of the energy changes occurring during the photocycle. A photocalorimetric method is clearly necessary to attack this problem, since we are dealing with a photoinduced process. Direct photocalorimetry has been used successfully to study a similar problem in the rhodopsin system (3–5), while data on the bR photocycle have been obtained by flash calorimetry (6). As the system is not affected irreversibly by strong light intensities, we thought that photoacoustic (PA) methods, which currently require strong illumination, could be used.

Most applications of photoacoustic spectroscopy (PAS) have been directed towards the investigation of absorption characteristics of highly scattering materials, taking advantage of the fact that this method is much less sensitive to light scattering than conventional absorption spectroscopy, owing to the nature of the photoacoustic effect (7) (see below). A basic assumption in these studies was that the measured PA signal is proportional to the amount of light absorbed. Relatively less attention has been paid to cases where part of the absorbed energy is stored in the system as photointermediates and photochemical products, dissipated as luminescence, or converted into electricity in photovoltaic processes (8–10). Here we use PAS to obtain information on thermodynamic and kinetic properties of the intermediates formed in the bR photocycle. Specifically, we calculate the wavelength dependence of heat dissipation to identify regions with varying photoactivity and to estimate values for energy stored by photoactivity; we determine the modulation frequency dependence of the PA signal to obtain the chronology and extent of heat changes during the photo-

cycle; and we determine rise and decay times of photointermediates. Procedures for calibrating and choosing proper references for the PA data and their analysis are discussed in detail. Limitations of the applicability of dissipation and frequency spectra are pointed out.

The values obtained for the enthalpy changes during the photocycle and for the characteristic decay times of the intermediates associated with them are found to depend significantly on the pH and ionic strength of the purple membrane suspensions. Some of these dependencies are interpreted in terms of the effect of pH and/or salt concentration on conformational changes of the protein-retinal complex in the membranes. The occurrence of conformational changes in light-adapted bR, during the photocycle, and especially upon formation of the L and M intermediates, was deduced, *inter alia*, from near-ultraviolet and visible absorption spectra of PM preparations, and was interpreted as movement of aromatic amino acid residues of bR, which might occur because the close packed helices which make up the protein move apart (11). Further evidence has been accumulating (2) and includes systematic observations of light-induced uptake or release of membrane-Bohr protons (which always accompanies the pumping process) (12), and light-induced conductivity changes in PM suspensions (13). These conformational changes seem to be much slower than the photocycle per se, and may well be associated with enthalpic changes detectable by PA calorimetry.

METHODS AND MATERIALS

Photoacoustic Data

In the PA method a sample situated in a closed chamber is illuminated by a beam of light modulated (or chopped) at an acoustic frequency. The heat generated in the sample by absorption of light is modulated at the same frequency and induces, in turn, a pressure wave in the surrounding medium. This wave is sensed by a suitable detector (usually a microphone), amplified, detected by a lock-in amplifier, and recorded (7, 14).

The experimental set up used for photoacoustic detection in this study is a further development of one described previously (15, 16). The light source was a 450-W xenon lamp, modulated by a mechanical chopper at a frequency that could be continuously varied between 15 and 400 Hz. The chopped beam was passed through a monochromator (500-nm blaze grating) driven by a DC motor (Bausch & Lomb Inc., Rochester, N.Y.). Two sets of slits were used, allowing wavelength resolution of either 5 or 10 nm. The monochromatic light was directed onto the measuring cell by a light guide. The cell was an improved version of one reported previously (9) and described in detail elsewhere (17). In this cell a gas phase surrounds the sample to minimize the effect of direct light-induced volume changes (see Appendix). The output signal was amplified and fed into a lock-in amplifier (Ortholoc 9502; Brookdeal Electronics Ltd., Bracknell, Berks., England), which received a reference signal from the chopper. The lock-in output was recorded against wavelength, frequency, or time. The modulated light intensity in all wavelength spectra was ~100 W/m^2 unless otherwise indicated.

The light was filtered through a cut off filter (>417 nm) to eliminate second-order effects. The wavelength scan speed was usually 10 nm/min and the system response time 1 s. All photoacoustic data were corrected for the lamp and monochromator spectrum, and for background (~5–10%). Correction for the lamp spectrum was performed by normalizing the measured wavelength spectra according to the spectrum of carbon-black powder (assumed to have total, wavelength-independent, absorption). The signals were linearly dependent on the light intensity. The background was estimated on the assumption that the photoacoustic signal from a suspension of purple membranes at 750 nm is due completely to background. In this way we were able to measure the background in the presence of the sample. This was necessary because the value obtained was different from the background signal estimated from an empty cell.

In the modulation frequency spectra the modulated light intensity was ~250 W/m^2. The measuring wavelength was 565 ± 10 nm. The background was corrected by measuring the signal at 750 nm for each chopping frequency. This approach was essential since the signal-to-background ratio varied considerably with the frequency. The correction for that part of the frequency dependence not influenced by photoactivity is discussed later. Conventional transmission spectra were measured in a Cary 118 spectrometer (Cary Instruments, Fairfield, N.J.), and fluorescence data were obtained in a Perkin-Elmer Corp. (Norwalk, Conn.), model MPF-44A fluorimeter. In both cases an optical cell with a path length of 0.1 mm (Nippon Silica Glass Co. Ltd., Tokyo, Japan) was used.

Materials

H. halobium cells (M1 and R1 strains) were grown as described by Eisenbach et al. (18), and purple membrane fragments were isolated according to Oesterhelt and Stoeckenius (19). Measurements were performed at ambient (19–22°C) temperatures on aqueous suspensions of membrane fragments with optical densities of 30 cm^{-1} at 565 nm. These were buffered at pH 3.8, 7.0, or 9.9, with mixtures of 10 mM glutamic acid, 5 mM 3-(*N*-morpholino) propane sulfonic acid (MOPS), and 10 mM Tris. Bleaching with hydroxylamine was carried out as described by Oesterhelt and Stoeckenius (20). Our sources of chemicals were as follows: disodium fluorescein was obtained from Eastman Organic Chemicals Div., Eastman Kodak Co., Rochester, N.Y.; glutamic acid and methylene blue from BDH Chemicals, Ltd., Poole, England; and MOPS from Sigma Chemicals Co., St. Louis, Mo.

RESULTS AND DISCUSSION

Analysis of Photoacoustic Data A simplified energy balance equation that quantifies the PA signal (ρ) measured under given conditions was suggested by Malkin and Cahen (10) and can be written as

$$\rho = k \cdot [I/I_0(\omega, \lambda)] \left[1 - \sum_i \frac{\phi_i \, \Delta E_i(\omega, \lambda)}{Nhc/\lambda}\right], \quad (1)$$

where I/I_0 is the fraction of light absorbed by the thermally active layer at wavelength λ and angular chopping frequency ω, k is an instrumental constant, N is Avagadro's number, h is Planck's constant, c is the speed of light, and λ is the wavelength (Nhc/λ is the equivalent energy of incident light with wavelength λ). The term in brackets represents the fraction of light converted into heat; ϕ_i and ΔE_i are the quantum yield and internal energy[1] change, respectively, of any light driven process that stores energy for periods longer than $1/\omega$.

The depth of the thermally active layer, i.e., the thick-

[1]Since in liquid/gas phase experiments, both the relative volume and pressure changes are small (see Appendix), the heat produced or consumed will be similar to the internal energy and enthalpy changes.

ness of a solid or liquid sample contributing to a PA signal sensed in the gas phase outside it, is governed by the chopping frequency and the thermal diffusivity of the absorbing material, α. This depth is given to a first approximation by the thermal diffusion length μ, which is equal to $(2\ \alpha/\omega)^{1/2}$ (7). For dilute aqueous suspensions, μ will have values like 6.6 μm at 1 kHz or 66 μm at 10 Hz. Thus, very concentrated solutions and strong intensities are required for PA measurements, because the technique becomes, essentially, a thin-layer method.

We define as the dissipation spectrum a plot of $\rho/(I/I_0)$ vs. λ. As discussed before (10, 16), such a plot will have minimal values over wavelength regions of maximal photochemical activity and will approach a constant, wavelength-independent, value when these activities approach zero. A major problem in calculating the dissipation spectrum from the measured PA spectrum is the proper evaluation of the fraction of light absorbed by the thermally active layer. The quantity $I/I_0(\omega, \lambda)$ can be calculated as $1-10^{-\epsilon(\lambda)\cdot c\cdot\mu(\omega)}$ [$\epsilon(\lambda)$ being the molar extinction coefficient and c the concentration], provided that the optical density for a given optical path and the thermal diffusivity are known. Although thermal diffusivities are not always known, the value of α for any dilute aqueous suspension will be practically the same as that of water (0.0014 cm^2/s), and biological samples with high water content will have similar values of α (21). Furthermore, relatively large changes in α will give rise to small changes only in μ and the effect of I/I_0 will be even smaller. To test this point and to see whether sufficiently accurate values of I/I_0 can be calculated in this way we applied the above procedure to a model system, disodium fluorescein, which forms highly fluorescent solutions whose quantum yield is wavelength-independent over a wide exciting wavelength range (22). As the fluorescence of such solutions can be quenched by potassium iodide, it can be varied from ~0.9 (without KI) to nearly zero (with ~3 M KI). According to Eq. 1, the PA signal in the presence of a high concentration of quencher (ρ_Q) is equal to $k \cdot I/I_0$ and can be used as a direct *in situ* measure of the light absorbed in the thermally active layer.

Fig. 1 *A* shows absorption and PA spectra of quenched and nonquenched solutions of fluorescein. The dissipation spectrum of fluorescein was calculated from these data, either as ρ/ρ_Q or as $\rho/(I/I_0)$ (Fig. 1 *B*). In the second case, two values of α were assumed, 0.001 and 0.002 cm^2/s. According to Fig. 1 *B* the three sets of data are in very good agreement below 485 nm, which confirms the above prediction that I/I_0 (ω, λ) is relatively insensitive to the thermal diffusivity. Above 485 nm the calculated spectra deviate significantly from the measured one; this deviation can be ascribed partly to the very different light intensities applied in measuring PA absorption spectra and is discussed elsewhere (23). Here again, however, the two values assumed for α give practically the same result.

The fact that the experimental points can be fitted to a

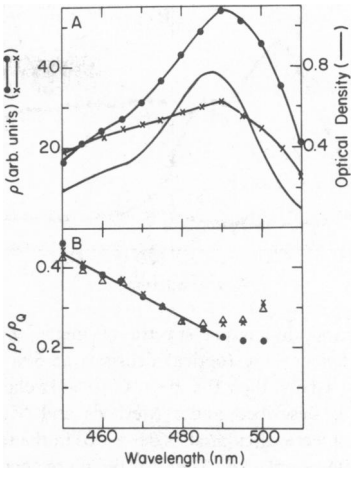

FIGURE 1 Spectra of disodium fluorescein. Fresh solutions of 1.7×10^{-3} M fluorescein in 0.01 M NaOH, with and without 3 M KI, were used. The quenched solution exhibited a fluorescence of <3% of the nonquenched one. (*A*) Solid line absorption spectrum (±KI); ●, PA spectrum of the quenched sample; x, PA spectrum of the nonquenched sample (×2.5). Chopping frequency: 40 Hz. (*B*) Dissipation spectra calculated either as ρ/ρ_Q (●) or as $\rho/(I/I_0)$. α was assumed to be either 0.001 cm^2/s (x) or 0.002 cm^2/s (Δ). The different sets of data were normalized to the same value at 475 nm.

straight line ($R > 0.99$) indicates that the product $\phi \cdot \Delta E$ is wavelength-independent. From the slope/intercept ratio, $\phi \cdot \Delta E$ can be calculated directly. This procedure is used by Cahen et al. (23) to obtain ϕ, as ΔE (average fluorescence emission wavelength) is known. Alternatively, if ϕ is known, ΔE can be calculated, as will be discussed below.

If all the incident light is absorbed in a depth shorter than the thermal diffusion length, the sample is photoacoustically saturated and will show peak flattening (24). This situation, considered a major obstacle in the application of PAS as an analytical tool, does not affect dissipation (or frequency) spectra, providing that the true value of I/I_0 can be substituted in Eq. 1. Fig. 2 illustrates this for two solutions of methylene blue. The solution in Fig. 2 *A* is the more dilute one and shows little, if any, PA saturation. In Fig. 2 *B* a 10-fold more concentrated solution was used and the PA spectrum is almost fully saturated. In spite of the large differences in the PA spectra, the dissipation spectra (calculated with the conventional transmission absorption spectrum of the less concentrated sample and by assuming $\alpha = 0.0014$) look very much the same. The wavelength independence of $\rho/(I/I_0)$ is typical when no photoactive processes occur ($\rho = k[I/I_0]$). The upward curving at the edges of the spectra may reflect a contribution of the background signal (17), which is pronounced only for low sample signals. The insert of Fig. 2 illustrates the danger when (I/I_0) is extrapolated from data for more dilute samples. In this case most of the solute in the true reference (concentrated sample) is present as dimers (25).

Although we can identify regions of different photochemical activity qualitatively from the dissipation spec-

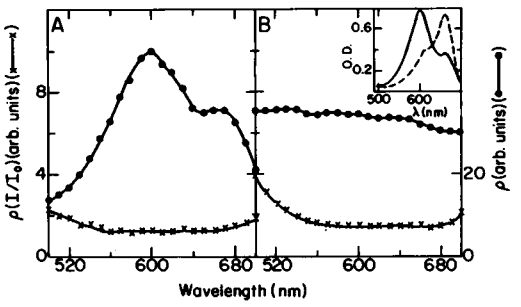

FIGURE 2 PA and dissipation spectra of methylene blue. Aqueous solutions of methylene blue (optical densities at 600 nm: 78 and 780 cm^{-1}) were prepared and their PA spectra (10.5-Hz chopping frequency) were measured as described under Methods and Materials (●). The dissipation spectra were calculated as described in the text (x). (*A*) Data for the more dilute sample. (*B*) Data for the more concentrated sample. The left scale in (*A*) is magnified 10-fold compared with that in (*B*). The insert shows the conventional (transmission) absorption spectra of the solution at 78 cm^{-1} measured in a cell with 0.1-mm length (solid line) and that of a 200-fold-diluted solution measured in a cell 1 cm in length.

tra, we may be hampered in our attempt to extract quantitative data by the occurrence of photoinduced optical absorption changes (e.g., bleaching) and by the presence of more than one chromophore with different photoactivities, as will be seen below. Information equivalent to that obtained from the dissipation spectra could in principle be extracted from conventional photocalorimetry. On the other hand, a unique application of PAS in studying photochemical processes uses its ability to measure the kinetics of heat production or consumption by a light-induced reaction taking place on a time scale of microseconds-to-milliseconds under physiological conditions. As discussed by Malkin and Cahen (10), such information can be obtained by following the frequency dependence of $\Sigma_i\ \phi_i\ \Delta E_i$. At high chopping frequencies only heat generated by fast reactions will be detected while at low frequencies heat generated both by fast and slow processes will contribute to the measured signal (9). Quantitative results can be obtained only if frequency effects on $\Sigma_i\ \phi_i\ \Delta E_i$ are separated from those on (I/I_0) and on the instrumental constant k. As shown above, we can use the slope/intercept ratio of the linear part in the dissipation spectrum for this. Alternatively we can measure at one wavelength only and try to find a reference that is identical to the sample but that is also photoinactive. For the work reported here, we found that a satisfactory reference could be prepared from a suspension of purple membrane, at the same concentration as the sample studied, bleached irreversibly with NH_2OH (20). Black ink was added to this to give it the same optical density at 565 nm as the sample containing bacteriorhodopsin. This preparation should have the same value of kI/I_0 (ω) as the sample studied, and since it is photochemically inactive the ratio between the two will be equal to $1 - \Sigma_i\ \phi_i\ \Delta E_i\ \lambda/Nhc$. It should be emphasized that any reference sample must have thermal properties identical to the measured sample, and a solution of black ink only, without bleached membrane fragments, was not satisfactory in this respect.

Fig. 3 *A* shows a frequency scan of the PA signals generated by suspensions of purple membrane and of bleached membrane fragments plus ink. The increase in signal observed upon reducing the chopping frequency down to 30 Hz mainly reflects the increase in thermal diffusion length. The decrease in signal under 30 Hz is due to decreasing microphone sensitivity below this frequency (17). This effect and the high noise introduced by the chopper at low frequencies limited accurate measurements to frequencies higher than 10 Hz.

The true frequency spectrum, i.e., a plot of $1 - \Sigma_i\ \phi_i\ \Delta E_i\ \lambda/Nhc$ vs. ω, is calculated as the ratio of the two curves and is shown in Fig. 3 *B*. As can be seen from this figure, the variations in $\phi\Delta E$ with ω are smaller and the relative dissipation increases by at most 30% upon reducing the frequency from 400 to 50 Hz. This effect is superimposed on a 10-fold larger increase in the PA signal owing to effects on I/I_0 (compare Fig. 3 *A* with 3 *B*). Obviously, under such circumstances precise determination of the true spectrum is very difficult; nevertheless, we were able to reproduce the characteristic behavior shown in Fig. 3 *B* repeatedly.

A potential artifact in PA detection of thermal dissipation is the possibility of volume changes in the solution resulting from light-induced reactions such as a change in the number of electrical charges. Such volume changes were measured for bacteriorhodopsin and interpreted in terms of light-induced protonation and deprotonation (6, 26, 27). On a priori grounds these volume changes are not expected to make a major contribution to the pressure

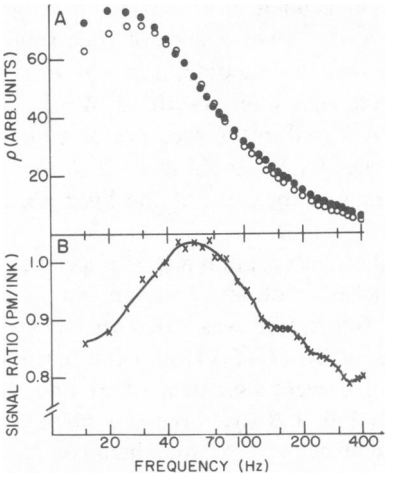

FIGURE 3 Frequency spectrum of bacteriorhodopsin. (*A*) PA signals of purple membrane fragments (○), buffered at pH 7.0, and of bleached membrane fragments to which black ink was added (●), were measured at 570 nm. The optical density in both cases was 30 cm^{-1}. (*B*) Signal ratio for curves similar to that in Fig. 5 *A*, but at pH 9.9. Similar results are obtained at pH 7.0. The signal ratio at high frequencies was calculated from measurements at five-fold higher sensitivity than shown in (*A*). For further details see Materials and Methods.

wave in the gas phase. This was confirmed by comparing the expected expansion in the gas phase due to heat production with that predicted by dissociation and association of protons during the photocycle. It turned out that the last effect should cause a volume change of <5% of that due to heating (see Appendix). The pH dependence of the frequency spectrum tends to confirm this, as shown below.

A further useful application of PAS is the ability to measure steady-state populations of photo-induced intermediates produced by an additional, continuous beam of light (16, 28). The sample can be excited by a strong continuous beam of light, which will populate photointermediates but will not interfere with the measurement (since only modulated pressure changes will be sensed by the lock-in amplifier). The advantage of PAS in this case is that the measurement is not limited to wavelengths different from those at which excitation is performed, and no detector saturation effects occur.

EXPERIMENTAL RESULTS

Dissipation Spectra of Bacteriorhodopsin

Fig. 4 shows the dissipation spectra obtained for preparations in which bacteriorhodopsin is the only pigment present. Both spectra exhibit similar features, which confirms our previous results (16, 28); they are, however, characterized by better signal-to-noise and signal-to-background ratios, owing to instrumental improvements.

Between 540 and 640 nm, the relative dissipation is a linear function of the wavelength, which indicates a constant value of $\Sigma_i\ \phi_i\ \Delta E_i$. This result confirms the reported wavelength independence of the quantum yield of M_{412} formation (29). We can now calculate the amount of energy that is not converted into heat as we did for fluorescein; in this case, however, all the energy not dissipated thermally is stored in the system, since the fluorescence of bacteriorhodopsin is marginal (30). At the red end of the spectrum the relative dissipation is higher than the value predicted by assuming a constant value of $\Sigma_i\ \phi_i\ \Delta E_i$ (dashed line). This behavior indicates a decrease in the quantum yield in this wavelength region. On the other hand, below 540 nm the system stores more energy than predicted by assuming a constant $\Sigma_i\ \phi_i\ \Delta E_i$. Although it is possible that either excitation to a second electronic level or light scattering effects[2] contribute to the decrease in thermal dissipation, the most likely explanation is absorption by photointermediates. The light intensities used in the PA and transmission experiments differ by a factor of ~10 (23) (dictated by signal/noise consideration in the PA experiments, where rather high light intensities are needed, and by spectral resolution in the transmission experiments). As we have shown earlier (16, 28), bleaching of the 570-nm absorbing species and accumulation of the absorbers at 412 and 660 nm occur when strong background light is used. To a small extent, the same will happen because of the strong measuring light (see Fig. 8, below). $\rho(I/I_0)$ will then yield values that are too large below 460 and above ~640 nm, whereas between 460 and 640 nm, values that are too small may be obtained. Measurement of PA and transmission (or reflection) spectra in the same setup can overcome this problem, but our present sample chambers are not yet suitable for this. Alternatively, we can use the PA spectrum at very low frequencies (<20 Hz) to obtain the absorption spectrum, assuming that at such frequencies the photocycle is complete and no energy storage is detected anymore. In our case poor signal-to-noise at low frequencies makes this method inaccurate, as does the fact that intermediates may decay on a time scale comparable to (chopping frequency)$^{-1}$. Therefore, we consider the information obtained from dissipation spectra as semiquantitative only.

A characteristic feature of the dissipation spectrum of bacteriorhodopsin is that the wavelength of minimal dissipation (~630 nm) is considerably red-shifted with respect to the wavelength of maximal absorption (565 nm). Evidently, it would be more efficient to excite the photocycle in the red tail (providing that the quantum yield does not drop too much) than in the wavelength of maximal absorption. Extrapolation of the complete linear portion of the dissipation spectrum to zero dissipation, to obtain the wavelength corresponding to $\Sigma_i\ \phi_i\ \Delta E_i$, leads to values

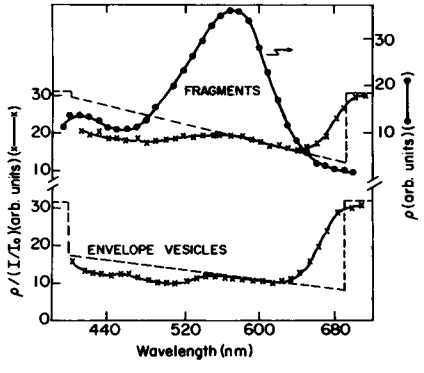

FIGURE 4 PA and dissipation spectra of bacteriorhodopsin. PA spectra of envelope vesicles and purple membrane fragments (in both cases the optical density at 565 nm was ~30 cm^{-1}) were measured at 40 Hz, as described in Materials and Methods. ●, PA spectrum of purple membrane fragments (with vesicles the same spectrum was obtained); x, dissipation spectrum; dashed line, hypothetical dissipation curve for a constant value of $\Sigma_i\ \phi_i\ \Delta E_i$ between 420 and 690 nm, with $\Sigma_i\ \phi_i\ \Delta E_i = 0$ outside this region.

[2]It is usually stated that PAS is insensitive to light scattering because only absorbed radiation is detected. In our case, however, some effect may result from the fact that light scattering can diminish the light intensity that reaches the chromophore. In this case, scattering will have an effect opposite to that found in conventional transmission spectroscopy. On the other hand, for a mixture of nonabsorbing spheres in an absorbing medium, an increase in PA signal, attributed to concentration of photons towards the surface, is found (31).

somewhat higher than expected (≥70% dissipation occurs, according to Lewis et al. [25] and Goldschmidt et al. [32]), namely between 5 and 40% energy storage of ~600 nm photons at modulation frequencies of 10 and 400 Hz, respectively. If we use the values at 460 and 640 nm only (around these wavelengths the differences in absorption characteristics due to different light intensities are minimal), we obtain more reasonable, lower values (~30% at 400 Hz), but at low frequencies extrapolation using only two wavelengths is too inaccurate. When the low-frequency (~10 Hz) data are used instead of transmission spectroscopic data to obtain dissipation values at these wavelengths (ρ/ρ [low freq.] instead of $\rho/[I/I_0]$), similar values for the fraction of stored energy are obtained. Obviously, large errors are involved in these extrapolations because of the rather small part of the absorbed photon energy that can be stored. In our case modulation frequency spectra, discussed below, provide a more reliable method to obtain energy storage data.

Significantly different dissipation spectra were obtained when intact *H. halobium* cells (strain R1) were measured (Fig. 5). This sample contains carotenoids whose spectrum overlaps to some extent that of bacteriorhodopsin and no information is available about any photochemical processes they may be involved in. The dissipation spectrum calculated from this preparation shows two main features: (*a*) a stronger decrease of $\rho/(I/I_0)$ with increasing λ than in Fig. 4, where most of the light is absorbed by bacteriorhodopsin, and (*b*) roughly wavelength-independent values of $\rho/(I/I_0)$ over the wavelength region in which the absorption is governed by the carotenoids (see insert in Fig. 5). This spectrum can be explained by assuming the existence of two overlapping chromophores, one of which stores part of the absorbed light and therefore shows wavelength dependence, while the other dissipates the total input as heat and thus gives rise to a wavelength-independent relative dissipation. The data summarized in Fig. 5, however, are not accurate enough to prove that all the light absorbed by carotenoids is dissipated thermally. All we can say at this stage is that according to the spectra in Fig. 5, much more light is stored by bacteriorhodopsin than by carotenoids, but the possibility of some storage by carotenoids (e.g., involving their triplet state, or energy transfer to bacteriorhodopsin) cannot be totally excluded. The wavelength dependence obtained in the region 560–670 nm is only partly due to energy storage by the purple membrane; it also reflects the increasing contribution of carotenoids to the total absorbance. Thus, in this case (two overlapping chromophores), such a line should not be used to estimate $\Sigma_i \phi_i \Delta E_i$.

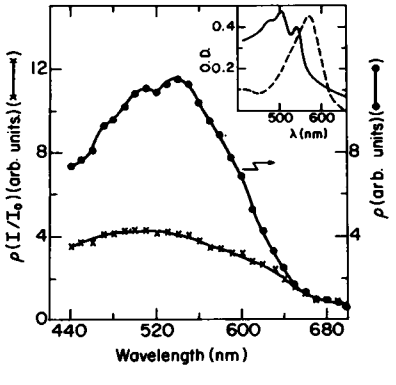

FIGURE 5 PA and dissipation spectra of *H. halobium* cells. Intact cells (strain R1) were spun down and measured as a fluffy pellet. ●, PA spectrum; x, dissipation spectrum. Chopping frequency: 40 Hz. Insert: conventional absorption spectra of carotenoids (solid line) and bacteriorhodopsin (dashed line). The carotenoid spectrum was obtained from cells grown in the absence of light and the bacteriorhodopsin spectrum is the difference spectrum between that of cells grown in the presence and absence of visible light.

Frequency Dependence of PA data

As discussed in the previous section, we can use the frequency dependence of the slope/intercept ratio of the line obtained from points at ~460 and 640 nm in the dissipation spectrum to obtain the corresponding values of the stored energy. In this manner, using ~10-Hz data instead of transmission spectroscopic data as described above, we could indeed estimate different amounts of stored energy at different frequencies: e.g., at 280 Hz the value for $\Sigma_i \phi_i \Delta E_i$ so obtained was 40(±20) kJ/mol, and at 160 Hz it was 30(±15) kJ/mol. Using the complete dissipation spectra and transmission spectroscopic data, we could estimate a value of 4(±10) kJ/mol for energy stored at 10.5 Hz. This behavior, the significance of which is discussed later, should be compared with that of fluorescein (23), where a frequency-independent value of ~225 kJ/mol for $\phi\Delta E$ is found. In addition to the problems of extracting quantitative data from dissipation spectra discussed above, this method becomes progressively less accurate as the frequency is decreased (low values of $\phi\Delta E$); for $\phi\Delta E = 0$, the slope is infinite, and as $\phi\Delta E \rightarrow 0$, small variations of the slope will cause large relative changes in $\phi\Delta E$.

The data obtained from dissipation can be compared to those shown in Fig. 3 *B*. Especially from these latter ones, we see that most of the absorbed light is dissipated thermally above 400 Hz (or in <400 μs, i.e., $1/[2\pi 400]$s). This agrees with results obtained by different methods. According to Goldschmidt et al. (32), the quantum yield on converting bR_{570} to K_{590} is 0.25–0.3. Thus, at least 70% of the absorbed energy should be converted into heat within <10 ps, well beyond our measuring range.

Fig. 3 *B* identifies at least four distinct events in which enthalpy changes take place. They are recognized as discontinuities of the experimental curve. Three of these events are exothermic processes and one, the slowest, is an endothermic process. Each process is characterized by a lifetime that can be estimated from the point of half-transition, and an enthalpy change that can be estimated from the relative size of the appropriate part of the curve

(the total amount of energy is known from the light intensity and the sample optical density).

In Fig. 6 we show the results obtained for two different pH values. The results at pH 7.0 and pH 9.9 (Fig. 3 *B*) are quite similar, whereas those obtained at pH 3.8 differ considerably. Such curves can be used to construct enthalpy schemes that contain the chronology of the enthalpy after absorption of light by bacteriorhodopsin (described in a preliminary communication [33]). Estimation of the lifetimes from the half-transition points yields semiquantitative values only as it is strictly applicable only to first-order reactions with well separated decay constants. In the case of a complex series of reactions occurring on a similar time scale, as in Fig. 3 *B*, precise kinetic analysis will require the assumption of kinetic models (10). Furthermore, the frequency spectrum describes the net enthalpy change, and different reactions occurring simultaneously cannot be distinguished, as all these reactions are sensed by their heat. Thus, the apparent disappearance of the endothermic event at low pH, for example, may represent enhancement of another exothermic event that occurs both at low and high pH. It should be noted that from the data presented here we cannot be certain whether the processes identified in Figs. 3 and 5 belong to a single chain of events (as we shall assume in our analysis below) or whether they represent alternative pathways in the photocycle whose occurrence is suggested by other spectroscopic measurements (34–36). Finally, the enthalpy change calculated for each event may be subject to a large experimental error owing to the very high background-frequency dependence, but this will not affect the discontinuities in the frequency spectrum.

Discussion of Frequency Dependence

In Table I we summarize results from several experiments for a number of preparations. The differences between the approximate lifetimes detected in the frequency spectra are quite small, and the values given in the table should be considered only as rough estimates. The three largest lifetimes found at pH 7.0 and pH 9.9 can be correlated with photointermediate decay times measured by modulation excitation spectroscopy (34): ~5 ms for O_{660}; ~2 ms for M_{412}, and ~0.8 ms for N_{530}. The lifetime of the event detected at ~290 Hz does not correspond to a known intermediate. The same holds for some of the events detected at pH 3.8, and in 200 mM KCl at pH 7.0; these may be related to intermediates that cannot be detected by absorption spectroscopy, and they may be related to conformational changes of the protein. The facts that the ~0.5-ms event is not detected in 200 mM KCl and that the ~1.3-ms intermediate appears only at low pH or in 200 mM KCl (whereas high pH does not seem to have an effect on the course of events) suggest that binding of positive ions to the predominantly negatively charged particles (2) is involved. Cation binding has also been

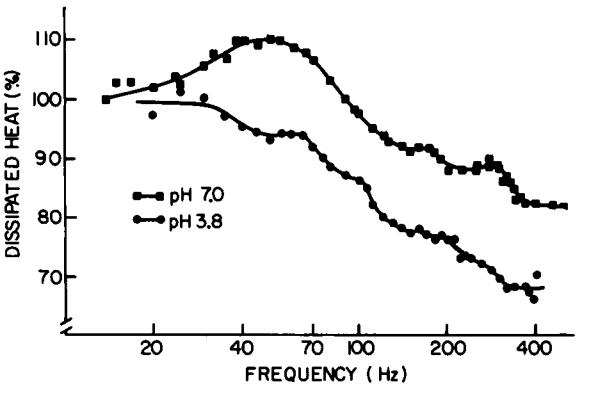

FIGURE 6 Frequency spectra (cf. Fig. 5 *B*) for purple membranes buffered in pH 7.0 (■) and pH 3.8 (●); measured as described in the legend to Fig. 3.

TABLE I
COMPARISON OF ENTHALPY CHANGES AND THEIR CHRONOLOGY FOR PURPLE MEMBRANE FRAGMENTS UNDER DIFFERENT CONDITIONS*

No added salt									+200 mM KCl		
pH 3.8			pH 7.0			pH 9.9			pH 7.0		
Frequency	τ‡	Dissipation§	Frequency	τ‡	Dissipation§	Frequency	τ	Dissipation§	Frequency	τ‡	Dissipation§
(Hz)	*(ms)*	*(%)*	*(Hz)*	*(ms)*	*(%)*	*(Hz)*	*(ms)*	*(%)*	*(Hz)*	*(ms)*	*(%)*
≥500	≤0.3	≤74	≥500	≤0.3	≤86	≥500	≤0.3	≤90	≥500	≤0.3	≤74
285	0.55	78	330	0.50	90	290	0.55	95	—	—	—
210	0.75	81	185	0.85	97	197	0.80	100	185	0.85	76
120	1.3	89	—	—	—	—	—	—	135	1.2	80
—	—	—	92	1.7	109	98	1.6	115	—	—	—
75	2.1	95	—	—	—	—	—	—	—	—	—
≤35	≥4.5	100	≤30	≥5.3	100	≤29	≥5.4	100	≤55	≥2.9	100

*From plots of frequency dependence of dissipated heat, with ink plus bleached purple membrane as reference.
Average values from several (3–5) experiments.
‡Approximate lifetime of intermediate. Estimated error: ≤10%.
§Percentage of input energy (212 kJ/einstein, 565-nm photon), dissipated as heat. Errors are highest at highest frequencies, owing to signal/noise problems. Estimated error at 500 Hz: ±10%; at ~100 Hz: ±2.5%.

adduced to explain light-induced conductivity changes in purple membrane suspensions (13).

The data from Table I were used to calculate the enthalpy changes connected with each step (Fig. 7). Here only the photons actually used in the photocycle were considered, and thus a background of 70% (32) has been subtracted. Although the total energy of a 565-nm photon is 212 kJ/einstein, 13% of this is released during vibrational relaxation and the true starting energy for the photocycle is taken as 184 kJ/einstein (~650-nm photon), on the assumption that tail absorption represents excitation to the lower vibrational level of the excited state.

As can be seen from Table I and Fig. 7, the endothermic final event reported earlier (33) is not found at low pH or in 200-mM KCl. This lends credibility to the suggestion that this step, too, is related to conformational changes of the protein-lipid complex. Such changes could lead to an increase in entropy of the system, and thus preserve the overall decrease in free energy necessary for a spontaneous process. Indeed, conformational changes of bacteriorhodopsin accompanied by alterations in the degree of exposure of protonatable groups to the medium have been demonstrated to occur under continuous illumination at any light intensity (2). An endothermic final event was also observed by Ort and Parson (6), who used a capacitor microphone calorimeter to determine volume changes, in both 14 and 200-mM KCl. The reason for the discrepancy between their results and ours at high ionic strength is at present unknown, but it should be stressed that the experimental conditions in the two types of experiments are quite different (e.g., illumination intensity per illumination period, frequency of illumination, and temperature). The differences in signal generation and detection between the PA and flash calorimetric methods are illustrated also by the pH dependence of the results, which allows a further check on the role of direct volume changes of the sample in the PA experiments. According to Ort and Parson (26), increasing the external pH from 7 to 9 should dramatically decrease the rates and increase the extents of all volume changes. Fig. 3 *B* shows the frequency spectrum obtained at pH 9.9. If we compare this curve with the pH 7.0 curve shown in Fig. 6, we see a striking similarity between the two (see also Table I). Obviously, events strongly dependent on the pH in this region cannot make a large contribution to these spectral features.

Increasing the KCl concentration influences the frequency spectra, but results in relatively small changes (the variation in the signal ratio with and without KCl was at most ±10%). According to Ort and Parson (27), 200 mM KCl should double the quantum yield of proton release during the photocycle. Hence, these results also support the assumption that volume changes do not contribute significantly to the measured PA signal.

PA Spectra of Photocycle Intermediates

Previously we have shown PA spectra of purple membrane fragments in which actinic light caused very small changes (16, 28). A much higher degree of M_{412} accumulation can be obtained in films of dried membranes (37). Fig. 8 shows photoacoustic spectra, taken in the presence and absence of actinic light, of membrane films equilibrated at a relative humidity of 63%. Even in the absence of actinic light, some population of M_{412} is generated by the measuring beam, which is strong compared with that used in conventional transmission spectroscopy (compare the PA and wavelength spectra), but in the presence of the continuous side illumination this is the main absorbing species. The spectrum of this species is similar to the one measured at low temperatures (11) and even the fine structure at ~430 nm (34) can be observed. As discussed above, in the section on Analysis of Photoacoustic Data, the measurement is not limited to wavelengths different from the

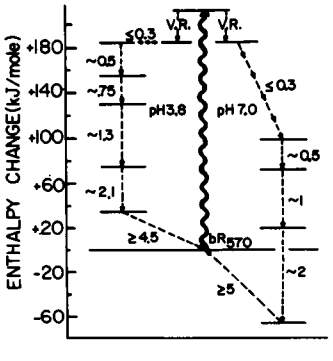

FIGURE 7 Scheme of enthalpy changes in purple membrane fragments at pH 3.8 and 7.0 (changes at pH 9.9 are similar), from data given in Table I, i.e., average values from several experiments. V.R., Vibrational relaxation to lowest vibrational level of excited state. Wavy thick arrow corresponds to excitation with 565 nm photons. Multiple arrows indicate possible occurrence of more than one intermediate, beyond our measuring limits. Numbers next to arrow refer to estimated lifetimes (in ms).

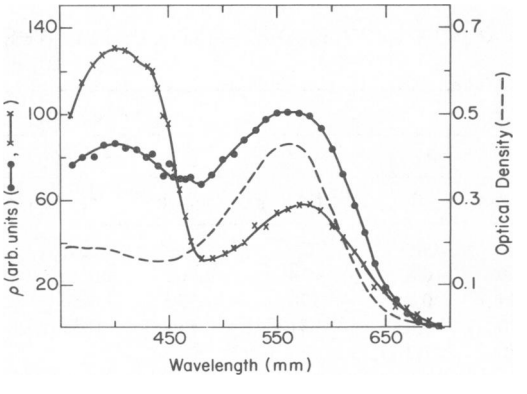

FIGURE 8 Spectra of dried films. Purple membrane fragments were dried in the sample holder of the measuring cells by a 48-h incubation in a large chamber at a relative humidity of 63%. PA spectra were measured at 40 Hz, with modulated light intensity of 5 W/m^2 in the presence (x) or absence (●) of continuous light ($\lambda > 460$ nm), the intensity of which was 1250 W/m^2. Dashed line, absorption spectrum of the dried film.

exciting one, and we could also examine the depletion of bR_{570} in the presence of actinic light at 570 nm.

Since the decay of M_{412} at low relative humidity is very slow (37), we were able to measure this process by following the rate of decrease in the PA signal at ~412 nm after the side illumination was turned off. The results are shown in Fig. 9. The decay can be fitted to a first-order process with a decay time of 10 s, which agrees with the expected lifetime (37) for the slowest process. The exact rise time of M_{412} under these conditions could not be calculated, since the measurement is limited by the response time of the present detection system (≥300 ms), which in its turn is dictated by signal-to-noise considerations. Nevertheless, we can put an upper limit of 1 s on the rise time of M_{412} under these conditions. For the bleaching of bR_{570} we found similarly a decay time of ~3 s. The buildup of this species has a characteristic time of ≤1 s under these conditions. Therefore, as is well known, other intermediates are involved between bR_{570} and M_{412}. These cannot be studied in the present setup, but it is quite possible that the use of difference spectra and more elaborate data analysis will make this possible in the future.

CONCLUSIONS

Our results show the occurrence of changes both in the amount of energy stored in intermediates of the photocycle and in their decay times as a function of pH and/or salt concentration. A slow endothermic step having a lifetime of ~5 ms, and a spectroscopically unidentified intermediate with a lifetime of ~0.5 ms, are particularly affected. These findings are interpreted in terms of alterations in cation binding to the protein-lipid complex, conformational changes of which are thought to be involved especially in the slow endothermic step.

Previous kinetic studies (12) have indicated that substantial movements of charged residues, accompanied by binding and release of up to three or four protons per mole of bR according to conditions, apparently occur during steady-state pumping. The association and dissociation of these protons (membrane-Bohr protons) is strongly affected by pH and ionic strength (38). It was suggested that fast conformational changes accompany energization of the photocycle (11) on illumination of light-adapted bR, and that these might result in a cascade of further changes with progressively increasing time scales (2). The latter probably relate to regions of the protein distal to the retinal chromophore. At present, it is not possible to correlate specific enthalpy changes, as calculated from our frequency spectra, with binding or release of membrane-Bohr protons, or movements of specific parts or residues on the protein, but some of our observations undoubtedly reflect these effects. It is hoped that by combining experimental results such as those reported here with those obtainable by other techniques (such as the use of fluorescence probes, whose results can be interpreted on the molecular level), more specific interpretations can be attained. Work in this direction is currently in progress.

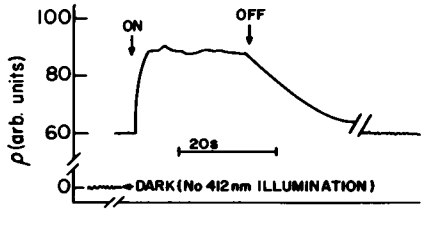

FIGURE 9 Light-induced signal changes. The change in the PA signal at 412 nm, upon turning the actinic light on and off, was recorded. Conditions as in Fig. 8.

APPENDIX

Rough Estimates of Expected Temperature and Volume Changes During the PA Experiments

We calculate the expected changes for our experimental conditions and compare the heat-induced volume changes with those expected from association and dissociation of protons (26, 27), and show that the latter processes will contribute in a minor way only to our PA signals.

Typical experimental conditions are: modulation frequency of 40 Hz, equal-duty cycle; incident-light intensity of 200 W/m^2, and samples with 30 cm^{-1} optical density. At 40 Hz the thermal diffusion length of a sample with a thermal diffusivity of $\sim 1.1 \times 10^{-3} cm^2/s$ (an average for several biological solutions as given in Touloukian [21]) will be 3×10^{-3}cm (7). Over this length, our samples will absorb ~20% of the incident light, most of which is converted to heat (70% after 10 ps) (32). The illumination area is 25 mm^2 (17), i.e., 5×10^{-3} J/s of light will reach the sample. At 40 Hz a single illumination period lasts 12.5 ms and, since only 20% of the incident light is absorbed, the energy input during that period is 1.25×10^{-5} J, or 3×10^{-6} cal.

The volume of the thermally active layer is 0.75 μl, and if we take as density 1.1 g/ml and as specific heat 0.75 cal/g-degree (averages between pure water, aqueous salt solutions, and glycerol), we find a temperature change of 4.8×10^{-3}°C/period in this volume. If the heat transfer efficiency to the gas phase is 1, this number gives the maximal temperature increase of the gas phase adjacent to the sample.

At 40 Hz the thermal diffusion length of air is 0.39 mm, from which we find the gas volume that can react in-phase to heat changes in the suspension as $0.39 \times 25 = 9.7$ μl. If the ambient temperature is 300°K, the calculated temperature rise will cause a maximal expansion of 1.5×10^{-4} μl/period in this gas phase volume.

In estimating the expected volume change due to protonation or deprotonation of the Schiff base (26, 27), we have to consider the whole suspension rather than the thermally active layer alone, because volume changes will be transmitted much more rapidly than heat changes. Thus, nearly all of the incident light will be absorbed and deprotonation to the extent of about 0.3 H^+/(photon absorbed) will occur. This process takes place in ~1 ms, during which period 1.4×10^{13} photons will be absorbed, producing 7×10^{-12} moles of charges. The actual volume change caused by this process depends on the buffer capacity and type of buffer present in the suspension (26). Since we use very concentrated suspensions, we can assume that they are highly buffered by the phospholipid head groups in the membrane, which will lead to a volume change that may be equal to (but is probably less than) that obtained with free phosphate, i.e., ≤24 ml/mol (39). From this we arrive at an expected maximum volume change, owing to deprotonation, of $\sim 1.7 \times 10^{-7}$ μl (both in the

suspension and in the gas phase). Since this volume change develops during 1 ms, however, its full effect will also be observed at modulation frequencies higher than 40 Hz, when the thermal diffusion length, and thus the heat-induced volume change, is much smaller than at 40 Hz. If we repeat the above calculations of the heat-induced volume change for a modulation frequency of 500 Hz (1-ms illumination period) a temperature increase of 0.38×10^{-3}°C is found, which results in a maximum volume change of 0.3×10^{-5} μl in the gas phase. Even under these conditions, the predicted volume change due to protonation is only 5% of that predicted from the thermal effect.

We can also attempt to calculate the expected volume changes due to deprotonation, using the values reported by Ort and Parson (26, 27), and try to adapt them to our experiment. Such calculations involve certain assumptions since the experimental conditions in the two cases are very different. The maximum volume change obtained from purple membrane fragments suspended in 200 mM KCl plus 5 mM phosphate (pH 7.8) at 2°C, and illuminated at 5.7×10^{-9} einstein flash is 5.4×10^{-5} μl (cf. Fig. 2 in Ort and Parson [27]). If we assume that all the photons in the flash are absorbed (no information is given on sample flash-illuminated areas in the above reference), and if we assume that in this range of light intensities, the volume change depends linearly on the light intensity, we calculate a change of 2.2×10^{-7} μl in the volume at a light intensity of 2.3×10^{-11} einstein (this is the intensity during a single illumination period at 500 Hz in the PA experiment). This result will, however, depend considerably on experimental conditions; e.g., if the purple membrane fragments are suspended in H_2O rather than in KCl, and the pH is 7 instead of 7.8, decrease in volume change is to be expected on both counts (Fig. 5 in Ort and Parson [27] and Fig. 3 in Ort and Parson [26][3]).

Thus, here too we estimate a volume change of $\sim 10^{-7}$ μl owing to deprotonation of the Schiff base. We have assumed that any proton release from the membrane will bind to a phosphate group, which will give the maximal effect. Should part of the protons bind to the Tris buffer, which is present in the PA experiments at 10 mM, a considerably smaller change would be expected (Ort and Parson [26], Table I; Ort and Parson [27], Table I).

We thank C. P. Bean and J. LeGrange for their critical readings of the manuscript, and Knowles Electronics Inc., Franklin Park, Ill., for microphones.

This work was supported in part in the U. S.-Israel Binational Science Foundation, Jerusalem, Israel, and by the Kernforschungsanlage, Jülich, F. R. G., through the Israel National Council for Research and Development.

Received for publication 1 May 1980 and in revised form 4 June 1981.

REFERENCES

1. Stoeckenius, W., R. H. Lozier, and R. A. Bogomolni. 1979. Bacteriorhodopsin and the purple membrane of halobacteria. *Biochim. Biophys. Acta.* 505:215–278.
2. Eisenbach, M., and S. R. Caplan. 1979. The light-driven proton pump of *Halobacterium halobium:* mechanism and function. *Curr. Top. Membr. Transp.* 12:165–248.
3. Cooper, A., and C. A. Converse. 1976. Energetics of primary processes in visual excitation: photocalorimetry of rhodopsin in rod outer segment membranes. *Biochemistry.* 15:2970–2978.
4. Cooper, A. 1979. Energetics of rhodopsin and isorhodopsin. *FEBS (Fed. Eur. Biochem. Soc.) Lett.* 100:382–384.
5. Cooper A. 1979. Energy uptake in the first step of visual excitation. *Nature (Lond.).* 282:531–533.
6. Ort, D. R. and W. W. Parson. 1979. Enthalpy changes during the photochemical cycle of bacteriorhodopsin. *Biophys. J.* 25:355–364.
7. Rosencwaig, A. 1980. Photoacoustics and photoacoustic spectroscopy. John Wiley & Sons, New York.
8. Harshbarger, W. R., and M. B. Robin. 1973. The opto-acoustic effect. Revival of an old technique for molecular spectroscopy. *Accounts Chem. Res.* 6:329–338.
9. Hunter, T. F., and M. G. Stock. 1974. Photophysical processes in the vapour-phase measured by the optic-acoustic effect. II. *J. Chem. Soc. Faraday Trans. II,* 70:1022–1028.
10. Malkin, S., and D. Cahen. 1979. Photoacoustic spectroscopy and radiant energy conversion: theory of the effect with special emphasis on photosynthesis. *Photochem. Photobiol.* 29:803–813.
11. Becher, B., F. Tokunaga, and T. G. Ebrey. 1978. Ultraviolet and visible absorption spectra of the purple membrane protein and the photocycle intermediates. *Biochemistry.* 17:2293–2300.
12. Eisenbach, M., H. Garty, E. P. Bakker, G. Klemperer, H. Rottenberg, and S. R. Caplan. 1978. Kinetic analysis of light-induced pH changes in bacteriorhodopsin-containing particles from *Halobacterium halobium. Biochemistry.* 17:4691–4698.
13. Slifkin, M. A., H. Garty, W. V. Sherman, M. F. P. Vincent, and S. R. Caplan. 1979. Light-induced conductivity changes in purple membrane suspensions. *Biophys. Struct. Mech.* 5:313–320.
14. Pao, Y. H. 1977. Optoacoustic spectroscopy and detection. Academic Press, Inc., New York.
15. Cahen, D., E. I. Lerner, A. Auerbach. 1978. Simple setup for single and differential photoacoustic spectroscopy. *Rev. Sci. Instrum.* 49:1206–1209.
16. Garty, H., D. Cahen, and S. R. Caplan. 1978. Use of photoacoustic spectroscopy in the study of the bioenergetics of purple membranes. *In* Energetics and Structure of Halophilic Microorganisms. S. R. Caplan and M. Ginzburg, editors. Elsevier/North-Holland, Amsterdam. 253–259.
17. Cahen, D., and H. Garty. 1979. Sample cells for photoacoustic measurements. *Anal. Chem.* 51:1865–1867.
18. Eisenbach, M., S. Cooper, H. Garty, R. M. Johnstone, H. Rottenberg, and S. R. Caplan. 1977. Light-driven sodium transport in sub-bacterial particles of *Halobacterium halobium. Biochim. Biophys. Acta.* 465:599–613.
19. Oesterhelt, D., and W. Stoeckenius. (1974). Isolation of the cell membrane of *Halobacterium halobium* and its fractionation into red and purple membranes. Methods Enzymol. 31:667–668.
20. Oesterhelt, D., and W. Stoeckenius, 1971. Rhodopsin-line protein from the purple membrane of *Halobacterium halobium. Nature (Lond.)* 233:149–152.
21. Touloukian, Y. S., editor. 1970. Thermophysical Properties of Matter: The TPRC Data Series. IFI/Plenum Publishing Corp., New York.
22. Demas, J. N., and G. A. Crosby. 1971. The measurement of photoluminescence quantum yields. A review. *J. Phys. Chem.* 75:991–1024.
23. Cahen, D., H. Garty, and R. S. Becker. 1980. Photoacoustic photocalorimetry of concentrated fluorescent solutions. *J. Phys. Chem.* 84:3384–3389.
24. Somoano, R. B. 1978. Photoacoustic spectroscopy of condensed matter. *Angew. Chem. Int. Ed. Engl.* 17:238–245.
25. Lewis, G. N., O. Goldschmid, T. T. Magel, and J. Bigeleisen. 1943. Dimeric and other forms of methylene blue: absorption and fluorescence of the pure monomers. *J. Amer. Chem. Soc.* 65:1150–1154.
26. Ort, D. R., and W. W. Parson. 1978. Flash-induced volume changes in bacteriorhodopsin-containing membrane fragments and their relationship to proton movements and absorbance transients. *J. Biol. Chem.* 253:6158–6164.
27. Ort, D. R., and W. W. Parson. 1979. The quantum yield of flash-induced proton release by bacteriorhodopsin-containing membrane fragments. *Biophys. J.* 25:341–353.

[3]Direct calculation of the expected volume changes from these data is not possible, since the flash intensity used is not given.

28. Cahen, D., H. Garty, and S. R. Caplan. 1978. Spectroscopy and energetics of the purple membrane of *Halobacterium halobium*. *FEBS (Fed. Eur. Biochem. Soc.) Lett.* 91:131–134.
29. Becher, B., and T. G. Ebrey. 1977. The quantum efficiency for the photochemical conversion of the purple membrane protein. *Biophys. J.* 17:185–191.
30. Alfano, R. R., Y. W. Govindjee, B. Becher, and T. G. Ebrey. 1976. Picosecond kinetics of the fluorescence from the chromophore of the purple membrane protein of *Halobacterium halobium*. *Biophys. J.* 16:541–545.
31. Helander, P., I. Lundström, D. McQueen. 1980. Light scattering effects in photoacoustic spectroscopy. *J. Appl. Phys.* 51:3841–3847.
32. Goldschmidt, C. R., M. Ottolenghi, and R. Korenstein. 1977. The quantum efficiency of the bacteriorhodopsin photocycle. *Biophys. J.* 17:179–183.
33. Garty, H., D. Cahen, and S. R. Caplan. 1980. Photoacoustic photocalorimetry of *Halobacterium halobium* photocycle. *Biochem. Biophys. Res. Commun.* 97:200–204.
34. Slifkin, M. A., H. Garty, W. V. Sherman, and S. R. Caplan. 1979. Modulation excitation spectrophotometry of bacteriorhodopsin. *Int. J. Biol. Macromol.* 1:61–64.
35. Hurley, J. B., B. Becher, and T. G. Ebrey. 1978. More evidence that light isomerizes the chromophore of purple membrane protein. *Nature (Lond.).* 272:87–88.
36. Sperling, W., P. Carl, C. N. Rafferty, and N. D. Dencher. 1977. Photochemistry and dark equilibrium of retinal isomers and bacteriorhodopsin isomers. *Biophys. Struct. Mech.* 3:79–94.
37. Korenstein, R., and B. Hess. 1977. Hydration effects on the photocycle of bacteriorhodopsin in thin layers of purple membranes. *Nature (Lond.)* 270:184–186.
38. Klemperer, G., M. Eisenbach, H. Garty, and S. R. Caplan. 1978. The effect of salt on the light-induced pH changes in purple membrane from *Halobacterium halobium*. *In* Energetics and Structure of Halophilic Microorganisms. S. R. Caplan and M. Ginzburg, editors. Elsevier/North-Holland, Amsterdam. 291–296.
39. Neuman, R. C., W. Kauzmann, and A. Zipp. 1973. Pressure dependence of weak acid ionization in aqueous buffers. *J. Phys. Chem.* 77:2687–2691.